Geophysical Research Letters

RESEARCH LETTER
10.1029/2018GL080296

Key Points:
- A new turbulence velocity scale is introduced, valid for regimes driven by a combination of wind shear, Stokes drift, and buoyancy fluxes
- The new velocity scale is shown to collapse high-fidelity simulation results over a variety of conditions and regimes
- We propose a simple model that can accurately predict the vertical distribution of buoyant material, which is crucial to predict their fate

Supporting Information:
- Supporting Information S1

Correspondence to:
M. Chamecki,
chamecki@ucla.edu

Citation:
Chor, T., Yang, D., Meneveau, C., & Chamecki, M. (2018). A turbulence velocity scale for predicting the fate of buoyant materials in the oceanic mixed layer. *Geophysical Research Letters*, *45*. https://doi.org/10.1029/2018GL080296

Received 4 SEP 2018
Accepted 9 OCT 2018
Accepted article online 16 OCT 2018

A Turbulence Velocity Scale for Predicting the Fate of Buoyant Materials in the Oceanic Mixed Layer

Tomas Chor[1], Di Yang[2], Charles Meneveau[3], and Marcelo Chamecki[1]

[1]Department of Atmospheric and Oceanic Sciences, University of California, Los Angeles, CA, USA, [2]Department of Mechanical Engineering, University of Houston, Houston, TX, USA, [3]Department of Mechanical Engineering, The Johns Hopkins University, Baltimore, MD, USA

Abstract We introduce a general framework to predict the fate of buoyant materials in the oceanic mixed layer. The framework is based on the estimation of a turbulence velocity scale for the vertical mixing of buoyant materials. By combining this velocity scale with the material's terminal rise velocity and a K-profile parameterization, we are able to derive an analytical prediction for the vertical profile of material concentration that is shown to be a reasonably accurate and general representation for oceanic mixed layer regimes driven by various levels of wind shear, Stokes drift, and buoyancy flux. The analytically predicted profile allows us to estimate relevant parameters for the fate of buoyant materials, such as the depth of a plume's center of mass and the horizontal transport. We show that the predictions agree with large-eddy simulations driven by various combinations of wind shear, Stokes drift, and buoyancy fluxes.

Plain Language Summary The flow of the ocean near the surface is influenced by many different natural phenomena. The three most important are waves, wind, and the cooling of seawater. These influences make the ocean behave in very distinct ways, which is a challenge for investigators trying to understand and predict the fate of pollutants that may happen to be dispersed in the water (e.g., oil or plastic). In practice this means that it is difficult for investigators to know, for example, whether oil will form a slick at the surface or be mixed downward into the water column, or where the oil will be transported. We present a framework that is general enough to be valid over a wide range of conditions that are naturally found in ocean. With this framework it is possible to make predictions that hold over a more realistic general range of situations without the need for large computer simulations. We demonstrate its applicability by making hypothetical predictions for the transport and mixing of oil and comparing them with computer models of the same conditions, as well as applying it to data measured in the Gulf of Mexico.

1. Introduction

Predicting the fate of buoyant materials in the oceanic mixed layer (OML) is challenging for both numerical and theoretical studies. One issue is the very different dynamics associated with each of the main forcings in the OML (most notably wind shear, Stokes drift, and buoyancy fluxes) which have distinct effects on the fate of buoyant plumes (Chen et al., 2016, 2018; Liang et al., 2018; J. R. Taylor, 2018; Yang et al., 2014). This issue is aggravated by the lack of a reliable approach to generalize results across the different regimes that arise by the combination of these forcings (Zilitinkevich, 1994). For the case of noninertial particles, whose defining parameter is their terminal rise velocity, the challenge can be traced back to the lack of a general (i.e., appropriate for several forcing conditions) turbulence velocity scale with which to analyze results. The lack of a common velocity scale makes it difficult both to combine results from individual studies (which tend to focus on a subset of the forcings) and to translate them into realistic regimes in which different forcings are acting together. For instance, Yang et al. (2014, 2015) focused on the effect of Langmuir turbulence and used the Stokes drift velocity, Chor et al. (2018) studied particle plumes under free convection and used a convective velocity scale, and Kukulka and Brunner (2015) and Liang et al. (2018) studied the effects of Ekman and Langmuir turbulence and used the friction velocity. These velocity scales represent very different physical processes, and it is not clear how the conclusions of one study affect the others.

In this work we address this issue by defining a generalized turbulence velocity scale (W) for the vertical mixing of buoyant materials that is based only on bulk properties of the flow. Generalized expressions for a velocity scale to characterize flow dynamics under different forcing conditions have been sought in the literature, for example, by Large et al. (1994) and Zilitinkevich (1994) using Monin-Obukhov theory and by De Bruin and Bink (1994) using statistical measures of the flow. Our approach is to seek a turbulence velocity scale to characterize the mixing of buoyant materials specifically, instead of more general flow dynamics, which significantly simplifies the problem.

We demonstrate the applicability of W as an appropriate framework by deriving an analytical model to predict some key features of buoyant materials transport in the OML (section 2). As will be demonstrated, the main advantage of our model is the representation of the vertical material distribution with an expression that is valid over different combinations of forcing conditions, which is possible only because of the validity of W in a wide range of cases (correct representation of vertical material distribution is crucial in order to correctly determine the transport and spreading of plumes; Chen et al., 2018; Liang et al., 2018). We demonstrate the usefulness of the model by making comparisons with a set of numerical experiments using large-eddy simulation (LES) that span a range of forcing conditions (sections 3 and 4).

2. Theory

For the purposes of this work we model the materials as noninertial buoyant particles, which is a valid approximation for a range of particulate materials in the ocean, most notably oil and microplastic marine debris (Chor et al., 2018; Kukulka & Brunner, 2015). For these cases we can accurately express the velocity of the particles as (Chor et al., 2018; Yang et al., 2016)

$$\mathbf{v} = \mathbf{u} + w_r \mathbf{e}_3, \tag{1}$$

where $\mathbf{v}$ is the total particle velocity, $\mathbf{u}$ is the flow velocity, w_r is the material's terminal rise velocity, and $\mathbf{e}_3$ is the unit vector in the direction opposite to the gravitational force. With these assumptions each material is uniquely characterized by its terminal rise velocity w_r.

2.1. Turbulence Velocity Scale

Here we seek to estimate a general turbulence velocity scale W to which w_r may be compared in realizations of buoyant material dispersion in the OML under different forcing conditions. In order to establish a unique velocity scale, we consider the turbulent kinetic energy (TKE) budget equation in steady state, neglecting horizontal gradients, turbulent transport, and pressure effects:

$$0 = u_*^2 \frac{\partial \langle u \rangle}{\partial z} + u_*^2 \frac{\partial \langle u_S \rangle}{\partial z} + \langle w' b' \rangle - \epsilon, \tag{2}$$

where ϵ is the TKE dissipation rate, u_S is the Stokes drift velocity, $u_* = \sqrt{\tau_s/\rho}$ is the friction velocity (τ_s is the surface wind stress and ρ is the seawater density), b is the buoyancy, $\langle . \rangle$ is the horizontal average operator (assumed here to approximate a Reynolds average operator), and a primed variable denotes a fluctuation with respect to the horizontal average. We can approximate each of the terms as ratios between velocity scales and length scales:

$$\epsilon \sim \frac{W^3}{l_\epsilon}, \qquad \frac{\partial \langle u \rangle}{\partial z} \sim \frac{u_*}{l_s}, \qquad \frac{\partial \langle u_S \rangle}{\partial z} \sim \frac{u_{S_0}}{l_L}, \qquad \langle w' b' \rangle \sim \frac{w_*^3}{l_c}, \tag{3}$$

where $w_* = \left(B_0 \, |h|\right)^{1/3}$ is the Deardorff convective velocity (Kaimal et al., 1976; h is the OML depth and B_0 is the outward buoyancy flux at the surface), and u_{S_0} is the Stokes drift velocity at the surface. This produces

$$W^3 = u_*^3 \left(\kappa^{-3} + \frac{A_L^3}{La_t^2} \right) + A_c^3 w_*^3, \tag{4}$$

where $La_t = \sqrt{u_*/u_{S_0}}$, $A_L^3 = l_\epsilon / l_L$ and $A_c^3 = l_\epsilon / l_c$ are coefficients that represent, respectively, the contributions of Langmuir and convective turbulence to W, and $\kappa = 0.41$ is the Von Kármán constant (any constant of proportionality from equation (3) is absorbed into the coefficients of equation (4)).

In deriving equation (4) we also assume that $l_\epsilon / l_s = \kappa^{-3}$, such that in shear turbulence the relation reduces to $W = \kappa u_*$ (in agreement with the standard K-profile parameterization [KPP]). We also assume that the different forcings have negligible coupling with each other. Although this assumption may not be valid at times (e.g., convection could reduce the vertical shear for a given wind stress, while turbulence generated by wind shear might disrupt convective plumes), our results seem to support this idea for the cases studied here.

Finally, although there are no formal grounds to suggest that the ratios of length scales should be universal, fixing their values for the range of applications examined in this paper will be shown to produce good results (section 4). With the ratios fixed, coefficients A_L and A_c can be determined by obtaining W for two separate simulations. This process will be detailed in section 4, but we present the results here for completeness:

$$A_L = 0.816, \qquad A_c = 1.170, \tag{5}$$

which are the values used throughout the paper. Although this is similar to the approach used by Belcher et al. (2012) to estimate the TKE dissipation rate, using their fit directly in the present context produces poor results. This is mainly due to the significantly lower value of the coefficient for the wind stress when compared to other coefficients in our fit, which suggests that wind shear has a smaller influence on the vertical mixing of buoyant materials than on TKE production. Equation (4) is valid as long as the buoyancy flux at the surface is not stabilizing ($B_0 \geq 0$). In cases where $B_0 < 0$ the buoyancy flux acts to decrease TKE, and, although there have been investigations on vertical mixing under stabilizing buoyancy fluxes (e.g., Kukulka et al., 2013; Pearson et al., 2015), further research is needed in order to incorporate this effect in our approach.

2.2. Plume Predictions

In this section we use W to scale the eddy diffusivity and make analytical predictions later to be compared with numerical simulations. We start with the Eulerian conservation of particle mass for a homogeneous steady state flow averaged in the horizontal direction with no particle flux across the surface (Kukulka & Brunner, 2015),

$$\left\langle w'c' \right\rangle + w_r C = 0, \tag{6}$$

where $C(z)$ is the material concentration in steady state averaged in the horizontal direction, and c' is the fluctuation around it. We assume that the turbulent flux can be represented with a KPP formulation (Large et al., 1994) neglecting nonlocal contributions,

$$\langle w'c' \rangle = -W\,|h|\,G(z/h)\,\frac{\mathrm{d}C}{\mathrm{d}z}, \tag{7}$$

where W is given by equations (4) and (5) and $G(z/h) = (z/h)(1 - z/h)^2$. In the absence of Stokes drift, the eddy diffusivity $W\,|h|\,G(z/h)$ reduces to the same form given by Large et al. (1994) for the bulk of the OML.

Following the goal of simplicity, we refrain from modifying the shape of the KPP profile to account for the different forcing conditions. Instead, this information is condensed into W via its definition in equation (4). Motivated by equations (6) and (7), we define the floatability parameter β as

$$\beta = \frac{w_r}{W}, \tag{8}$$

which measures the tendency of turbulent mixing (characterized by W) to counteract the tendency of buoyant material to float upward (given by w_r). This is a generalization of the analogous parameter defined in Chor et al. (2018). Depending on the value of β, the buoyant material ranges from a flow tracer ($\beta = 0$) to a surface floater ($\beta \to \infty$; Chor et al., 2018).

Equations (6)–(8) can be combined to produce (note that $h < 0$ for the OML)

$$\frac{\mathrm{d}C}{\mathrm{d}z} + \frac{\beta}{h\,G(z/h)}C = 0,$$

which can be integrated to obtain an analytical solution for $C(z)$ as (Kukulka & Brunner, 2015)

$$C(z) = C_0 \left(\frac{1 - z/h}{z/h}\right)^{\beta} \exp\left(\frac{-\beta}{1 - z/h}\right) \qquad \text{for} \quad h \leq z \leq z_c, \tag{9}$$

where C_0 is a constant used to enforce $\int_h^{z_c} C\,\mathrm{d}z/|h - z_c| = 1$. Here z_c is a cutoff depth that marks a point were other physical processes not considered in equation (6) become important, and it should not impact results provided it is small enough. Since an accurate expression for $C(z)$ in the interval $z_c < z \leq 0$ would necessarily include these other processes, we make no attempt to describe the concentration in this range of z. Processes that could be considered when setting the value of z_c include diffusion, breaking waves, and slick formation (in the case of oil). Note that the relevant physical processes (and therefore the value of z_c) may depend on the choice of material to be studied.

As will be shown in section 4, $C(z)$ captures the overall features of vertical mixing rather well, even though the precise shape of individual profiles may not be represented with full accuracy. Equation (9) is relevant because it is a closed-form analytical solution that, as will be shown later, produces good results for a wide range of combinations of Langmuir, shear, and convective turbulence (due to the wide range of validity of the floatability parameter β). Thus, predictions made using equation (9) are, in principle, valid for a wide range of realistic conditions observed in the ocean.

As a bulk measure of the vertical mixing implied by $C(z)$, we can estimate the normalized depth of the plume's center of mass $\sigma_{cm} = h^{-1} \int_h^{z_c} z\, C(z)\, dz / \int_h^{z_c} C(z)\, dz$ with an approximated expression as

$$\sigma_{cm} \approx \begin{cases} \frac{1}{2} \frac{2\sin(\pi\beta)+5\pi\beta(\beta-1)}{2\sin(\pi\beta)-5\pi\beta} & 0 \le \beta < 1 \\ 0 & \beta \ge 1, \end{cases} \tag{10}$$

which will be used throughout this work. A detailed derivation of equation (10) from equation (9) can be found in the supporting information Text S1.

One of the main large-scale consequences directly controlled by the vertical distribution of material is the horizontal transport. A plume's center of mass with average vertical distribution $C(z)$ is horizontally advected with a velocity $\mathbf{U}_h$ that can be approximated by

$$\mathbf{U}_h = \frac{1}{|h - z_c|} \int_h^{z_c} C_0 \langle \mathbf{u}_h \rangle \left(\frac{1 - z/h}{z/h} \right)^{\beta} \exp\left(\frac{-\beta}{1 - z/h} \right) dz, \tag{11}$$

which neglects horizontal transport by turbulence. Here $\mathbf{u}_h$ is the total horizontal flow velocity (including the Stokes drift). From equation (11) we have that for flow tracers $\mathbf{U}_h$ is analogous to the Ekman transport, while for surface floaters the center of mass moves following the flow velocity at the surface, as observed in the simulations of Chen et al. (2018).

3. Numerical Setup

We use a LES model to investigate the analytical predictions in section 2. The model was already extensively described and used in several other investigations (Chor et al., 2018; Yang et al., 2014, 2016). Detailed information on the LES model and the simulation setup can be found in Text S2 of the supporting information (Bou-Zeid et al., 2005; Chamecki et al., 2008; Craik & Leibovich, 1976; Donelan & Pierson, 1987; Lilly, 1967; McWilliams & Restrepo, 1999; McWilliams et al., 1997; Smagorinsky, 1963).

All simulations presented here have a value for the Coriolis frequency of $f = 7 \times 10^{-5}$ s^{-1} and used a total of eight different cases of buoyant materials (modeled as sets of particles) characterized by rise velocities $w_r = 0$, 2.0×10^{-4}, 8.5×10^{-4}, 3.5×10^{-3}, 7.5×10^{-3}, 1.5×10^{-2}, 3.0×10^{-2}, and 5.5×10^{-2} m/s (these correspond to a passive tracer and oil droplets rising in water of diameters between 0.05 and 1.5 mm, Zheng & Yapa, 2000, and also fall in the range of observed values for microplastic, Kukulka et al., 2016). Five simulations were run using a 400-m horizontal and 120-m vertical domain length (which we name $S_1, S_2, \dots, S_5$), and the relevant parameters are given in Table 1. Thus, as can be seen in Table 1, the simulations span a wide range of conditions dominated by different forcings. It is worth mentioning that simulation S_4 is configured to match the peak of the joint probability density function of the Stokes drift, wind shear, and surface buoyancy flux according to Belcher et al. (2012), thus being the most representative case we can run with our LES model.

Figure 1 shows snapshots of material concentrations from three of the simulations in which the distinct dynamics become clear: S_2 (left column) is dominated by convective plumes, S_3 (middle column) is more uniformly mixed only by the surface shear, and S_4 (right column) is dominated by Langmuir turbulence.

We have also run two extra simulations that are identical to simulations S_3 and S_4 except for the boundary conditions for the buoyant materials (which we denote E_3 and E_4). While in simulations S_n the particles recirculate in a closed periodic domain until they are horizontally homogeneous, in simulations E_n we use the Extended Nonperiodic Domain LES for Scalar transport (ENDLESS) approach (Chen et al., 2016, 2018), which allows us to simulate plumes that are much larger than the flow domain. This is done by simulating the turbulent flow on an affordably small horizontal domain with periodic boundary conditions. The velocity field is then replicated periodically to cover much larger scales while it advects the buoyant material. Thus, with the ENDLESS approach a finite-sized plume can be realistically modeled, which allows us to accurately quantify the long-range horizontal transport.

Table 1
Parameters for the Simulations Used in This Paper

Simulation	u_* (m/s)	U_{10}(m/s)	w_* (m/s)	La_t	W (m/s)	h (m)	Domain type	$\Delta z/\lvert h\rvert$	Short description of forcings
S_1	0.01	8.1	0	0.3 (DP87)	0.021	−69.8	Periodic	7.2×10^{-3}	Wind stress + Stokes drift
S_2	0	0	0.019	–	0.022	−82.3	Periodic	6.0×10^{-3}	Buoyancy flux
S_3	0.01	8.1	0	∞	0.004	−69.3	Periodic	7.2×10^{-3}	Wind stress
S_4	0.007	5.9	0.009	0.3 (DP87)	0.016	−58.3	Periodic	8.6×10^{-3}	Wind stress + Stokes drift + Buoyancy flux (in a typical combination for the ocean)
S_5	0.007	5.9	0.009	0.5 (MS97)	0.013	−55.2	Periodic	9.0×10^{-3}	Wind stress + Stokes drift + Buoyancy flux (Stokes drift decoupled from the wind)
E_3	0.01	8.1	0	∞	0.004	−69.3	ENDLESS	7.2×10^{-3}	Same as S_3
E_4	0.007	5.9	0.009	0.3 (DP87)	0.016	−58.3	ENDLESS	8.6×10^{-3}	Same as S_4

Note. DP87 and MS97 indicate that the Stokes drift was calculated according to the spectra in Donelan and Pierson (1987) and as in McWilliams et al. (1997), respectively. U_{10} is the wind velocity at 10 m corresponding to u_*. All simulations have a vertical resolution of $\Delta z = 0.5$ m.

4. Results

4.1. Vertical Mixing

We first consider the determination of the coefficients of equation (4). The first step was to calculate the center of mass σ_{cm} for each different set of materials for simulations S_1 and S_2 only. Using these results, we fitted two optimal values of W (one for each simulation) against the analytical prediction given by equation (10). With two equations and two unknowns (from equation (4)) we were able to determine the coefficients A_L and A_c. The results were already given in equation (5), and we can see how they collapse estimates for σ_{cm} in Figure 2d. The fit was performed only for σ_{cm} in S_1 and S_2, and all other results follow with no further fitting.

It is clear from the organization of the points in Figure 2d that β is able to properly collapse the results for σ_{cm}. Results from simulation S_2 somewhat deviate from others, which is caused by the distinct dynamics between convective turbulence (dominant mechanism in S_2) and shear turbulence (dominant mechanism in the other simulations). Note that in Figure 2d the values for the coefficients A_L and A_c (and subsequently the values for β) are used to scale the x axis only, while the y axis is simply calculated from the LES results. The theoretical prediction given by equation (10) is also plotted in the figure and shows good agreement with the measured points. Note in particular the validity of the prediction that the buoyant material is almost exclusively present at the surface (thus, $\sigma_{cm} \to 0$) for $\beta > 1$.

Figures 2a–2c show the results for groups of horizontally averaged material concentration profiles with similar floatability contained within the circles in Figure 2d (following the same color coding). It is clear that there are differences among the profiles within a group due to distinct turbulence dynamics. In order to predict individual curves accurately, nontrivial changes to the parameterization of the turbulent mass flux would be needed. However, even though the precise shapes of the profiles differ, the differences between profiles on distinct beta groups is much larger than those caused by different turbulent regimes within the same beta group (and thus with similar values of β). This explains the good agreement of Figure 2d.

Analytical profiles calculated with equation (9) for the average β value in each group are also plotted in Figures 2a–2c, respectively, as solid black lines for comparison (and indicated in Figure 2d as black squares). It is clear that $C(z)$ agrees with LES results within the variations seen in the simulations themselves. This means that the analytical solution given by equation (9), which only requires knowledge of β, yields a good first approximation to the vertical distribution of material over broad ranges of oceanic conditions. It is a significant achievement that a simple theory can collapse results for simulations with such different dynamics as can be seen in Figure 1.

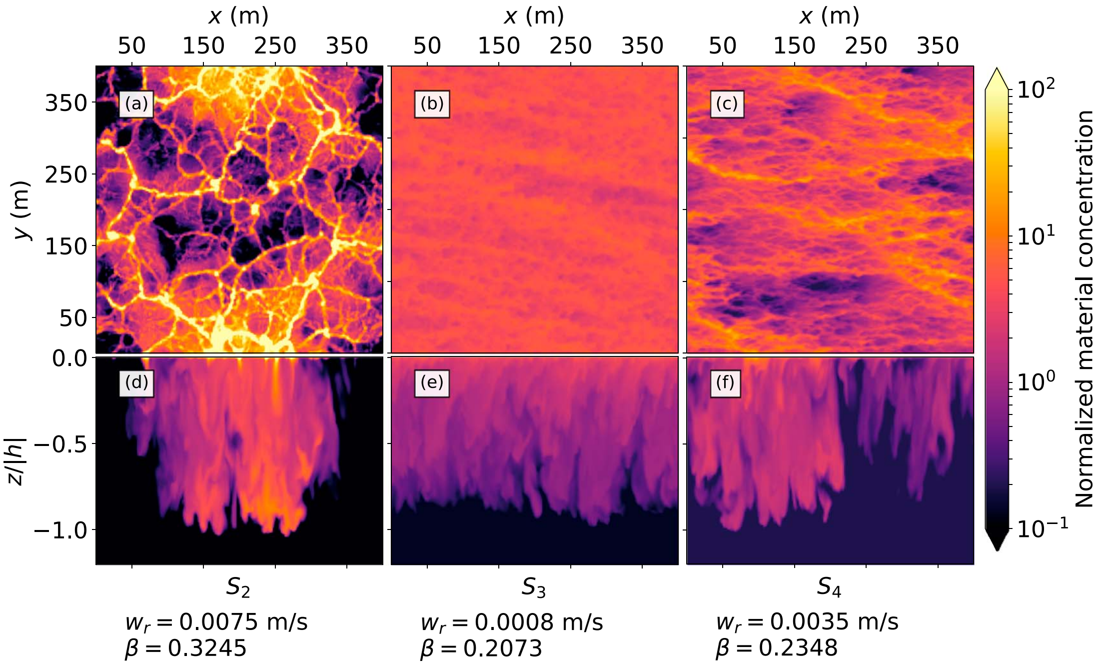

Figure 1. Instantaneous snapshots of concentration in simulations S_2, S_3, and S_4 (left, middle, and right columns, respectively). (a–c) The surface concentration and (d–f) the concentration in a vertical plane. Concentrations are normalized by their averages in the oceanic mixed layer. Horizontally averaged profiles for these cases are shown in Figure 2c.

4.2. Horizontal Advection

We proceed to use simulations E_3 and E_4 to assess predictions for the horizontal velocity of the center of mass $\mathbf{U}_h$ which are presented in Figure 3. Notice that the limit $\beta \rightarrow 0$ in Figure 3 corresponds to a nonbuoyant tracer (which is predicted to move with the vertical average of $\langle \mathbf{u}_h \rangle$ over the complete depth of the OML; vide equation (11)), while the limit $\beta \rightarrow \infty$ corresponds to a surface floater (which is predicted to be advected purely by the horizontal flow at the surface of the OML). Note also that for all cases considered in this work, the resolution of the data for $\langle \mathbf{u}_h \rangle$ was coarser than any appropriate choice for the cutoff scale z_c. Therefore, when calculating U_h from equation (11), the topmost data point for $\langle \mathbf{u}_h \rangle$ sets the upper limit of integration.

Results obtained by following the center of mass from simulations are plotted as points in Figures 3a and 3b for simulation E_3 and in Figures 3c and 3d for simulation E_4. Results obtained using equation (11) with the horizontal mean velocity $\langle \mathbf{u}_h \rangle$ from the LES are plotted as dashed lines in the same panels. There is overall good agreement between the predicted and measured transport velocities for both simulations. The fact that the shape of the curve is being well captured in both cases is a result of the profile given by equation (9) being successful in capturing the vertical mixing.

Notably, the estimate for $\mathbf{U}_h$ obtained using equation (11) with the LES velocity profile $\langle \mathbf{u}_h \rangle$ slightly underestimates the transport for $\beta > 0.3$ (thus, highly buoyant materials tend to move faster than the mean horizontal velocity of the surface flow). This is due to the fact that strongly buoyant materials tend to concentrate in regions of horizontal convergence at the surface (Chor et al., 2018). The results presented here indicate that these regions have faster-moving flow, a feature that has already been reported for Langmuir turbulence (Thorpe, 2004). Our results indicate that this effect is also true for wind-driven OMLs without Langmuir circulations. This effect on the horizontal transport cannot be predicted by equation (11) or any scheme that neglects horizontal turbulent transport and deserves future investigation.

For a completely predictive simple model, we evaluate $\mathbf{U}_h$ without needing to use LES to determine the profiles of $\langle \mathbf{u}_h \rangle$. For this purpose we determine the mean velocity from a one-dimensional (1-D) model

$$f\mathbf{e}_3 \times \langle \mathbf{u}_h \rangle = \frac{\mathrm{d}}{\mathrm{d}z}\left(\nu_e \frac{\mathrm{d}\langle \mathbf{u}_h \rangle}{\mathrm{d}z}\right), \qquad (12)$$
$$\nu_e(z) = \kappa u_* \, |h| \, G(z/h),$$

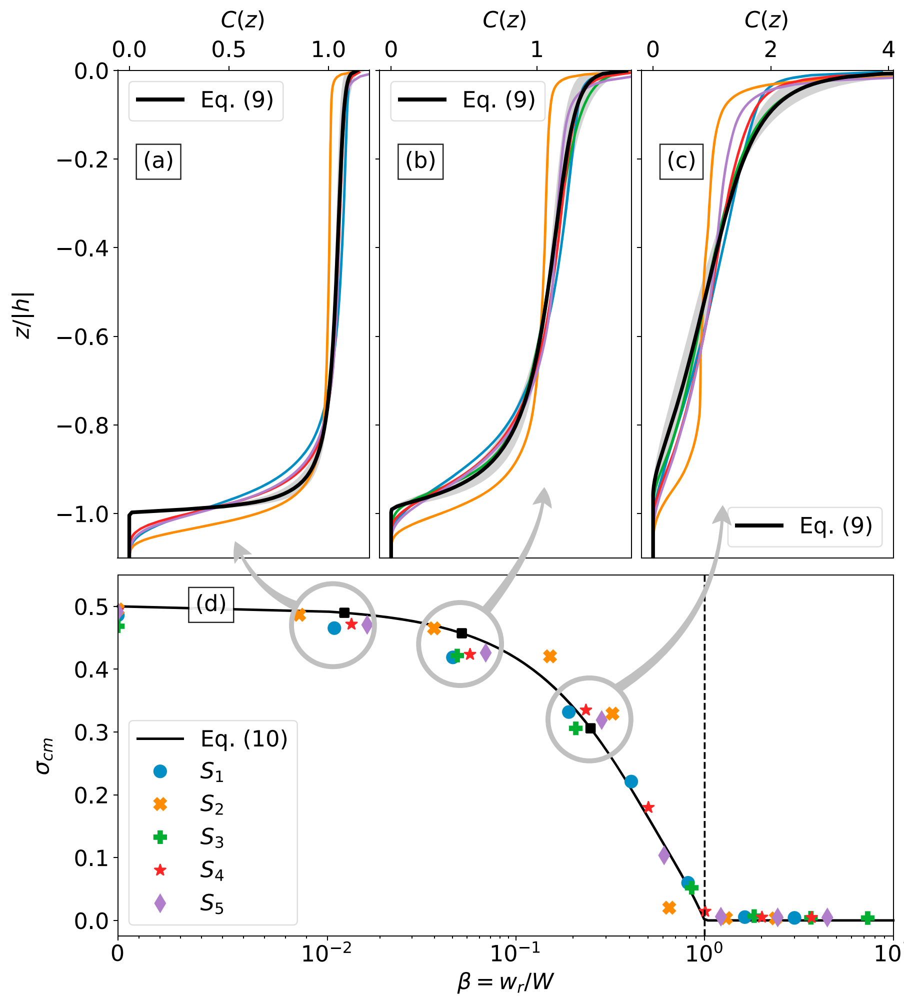

Figure 2. (a, b, and c) Vertical profiles of horizontally averaged material concentrations for cases contained within gray circles in panel d as colored lines along with the analytical predictions $C(z)$ (equation (9); black lines). The shaded gray area in these panels corresponds to the area defined by the predicted profile (equation (9)) using the minimum and the maximum values of β from the simulated cases for each panel. (d) Analytical prediction for the normalized center of mass (equation (10); black line) along with measured results from simulations (colored points). The leftmost part of panel d uses a linear scale, while the rest uses a logarithmic scale for the horizontal axis.

which is integrated numerically. In this model we do not use any information from the LES results (other than the depth of the mixed layer h) or from the material properties and floatability parameter β. Although we calculate the velocities with a sufficiently fine grid for grid convergence, we perform the integration in equation (11) using only the vertical grid points used by the LES to avoid mismatches due to different resolution of the quadrature. Results for this approach are plotted in Figures 3a–3d as solid lines. Once again there is reasonable agreement for both magnitude and direction. Estimates with the 1-D model tend to differ from simulations more than using $\langle \mathbf{u}_h \rangle$ from the LES model, which is expected since the 1-D model given by equation (12) ignores changes in the mean velocity from the different forcing conditions. Nonetheless, it is possible for the 1-D model to have better agreement than the LES-based model in some cases (e.g., in Figure 3c). We conclude that equation (11) along with the 1-D model in equation (12) is sufficient to reasonably predict the LES results for $\mathbf{U}_h$ with virtually no information from the simulations. Modifying the 1-D model used here (e.g., by modifying ν_e to account for Langmuir circulations and convection effects) can improve results for flow prediction and potentially improve the estimation of $\mathbf{U}_h$ (Large et al., 1994; McWilliams & Sullivan, 2000; Smyth et al., 2002).

We proceed to compare our 1-D model from equation (12) with the results presented by Liang et al. (2018) for the Langmuir-dominated case, shown in Figures 3e and 3f (information on this data can be found in Text S3 of

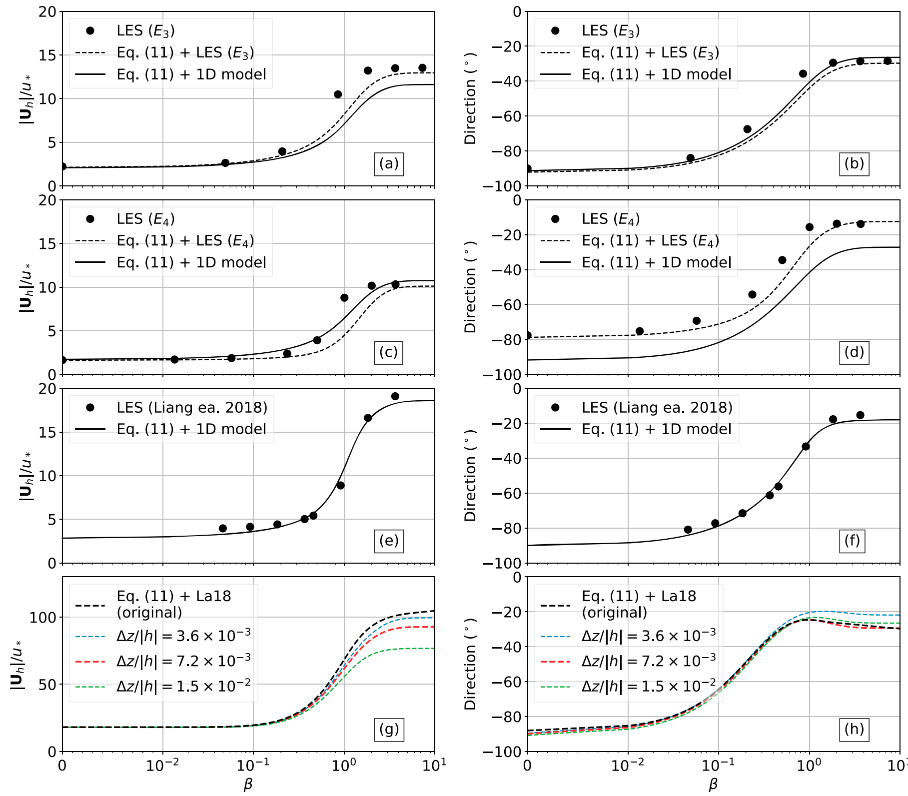

Figure 3. Measured and predicted results for the center of mass horizontal velocity $\mathbf{U}_h$. (left column) The magnitude and (right column) the direction of $\mathbf{U}_h$. (a and b) Simulation E_1. (c and d) Simulation E_4. (e and f) Results from the simulation performed by Liang et al. (2018). (g and h) Results from the measurements given in Laxague et al. (2018; denoted as La18). In all panels the points are results obtained only with LES, dashed lines results are obtained with equation (11) and the averaged velocity from the simulations (a–d) or field measurements (g and h), and solid lines are obtained with equation (11) using velocities from the 1-D model in equation (12). The colored dashed lines in panels g and h represent different coarse grainings of the original high-resolution data (Δz is the vertical resolution). LES = large-eddy simulation.

the supporting information). This case is similar to our simulation S_1 but with a considerably different steady state mixed layer depth of approximately 40 m. Again, there is good agreement with the 1-D model, with both the direction and magnitude being well captured.

Recently, Laxague et al. (2018) presented field observations that show large shear close to the surface, suggesting that numerical models must have very fine resolution to capture the correct transport direction of buoyant materials. Testing this hypothesis by simulating the conditions in which their measurements were obtained is beyond the scope of this work. However, we use their data along with our analytical predictions to assess the resolution of our simulations and the ability of LES in general to capture the transport of materials over a wide range of β. (Information about the data can be found in Text S4 of the supporting information.)

Results for $\mathbf{U}_h$ calculated using $\langle \mathbf{U}_h \rangle$ from the original data by Laxague et al. (2018) and equation (11) are shown in Figures 3g and 3h as black dashed lines. The red dashed lines show results for the same data coarse grained to match the median of the vertical resolutions used in our LES experiments ($\Delta z/|h| \approx 7.2\times10^{-3}$; see Table 1). Blue and green dashed lines show the same results for half and double this resolution, respectively. Figures 3g and 3h show that with our current resolution (dashed red lines) we are able to capture changes in $\mathbf{U}_h$ as a function of β. In the worst case, which is the limit $\beta \gg 1$, we underestimate $\mathbf{U}_h$ by $\approx$ 12% (due to the underestimation of $\langle \mathbf{U}_h \rangle$). The effects on the direction are less straightforward due to the variance of the velocity close to the surface exhibited by the observations; however, the error is always less than 10°. Overall, our analysis suggests that the vertical resolutions used in the simulations in this paper (corresponding to approximately 143 points in the OML) produce reasonable results, which adds more confidence to our simulation results.

5. Conclusions

We have introduced a generalized turbulence velocity scale W, which we used to define the floatability parameter β, leading to a simple analytical expression for the averaged vertical material concentration profile valid for a range of forcing conditions (equation (9)). Based on this expression, we derived predictions for the depth and horizontal advection velocity of a plume's center of mass with respect to β, which were then compared with LES results for a range of different oceanic regimes.

We showed that equation (9) is able to reproduce observed behaviors and represent the most important features of the phenomena investigated, and in this sense there was good agreement with the simulations. We also showed that a 1-D model for estimating the velocity yields reasonable results for the horizontal transport, allowing our analytical approach to be completely predictive. These results are particularly useful in the context of oil spills, where there is a large level of uncertainty concerning the application of chemical dispersants in the plume (Chen et al., 2018) and simple models such as the one presented here may be helpful. Furthermore, we obtained predictions for plume transport using field measurements of horizontal velocity from Laxague et al. (2018) which illustrate the impact of vertical resolution on the estimation of plume fate.

The framework presented here can also be used to determine other quantities of interest such as the horizontal effective diffusivity due to vertical shear, whose theoretical formulation was already demonstrated by Liang et al. (2018). With our framework it can be shown that the horizontal effective diffusivity scales with an inverse dependence on the solute's diffusivity as originally reported by G. I. Taylor (1953), and its calculation can be made applicable to general forcing conditions (details in Text S5 of the supporting information; Esler & Ramli, 2017; G. I. Taylor, 1953).

In summary, equations (4), (5), and (8)–(11) can be used to make predictions of mean transport speed, direction, and horizontal diffusion of buoyant plumes without the need of performing simulations with buoyant materials. Although it is preferred to have horizontal velocities from regional models or measurements for better results, reasonable estimates can still be obtained by using the 1-D model given in equation (12) if high-resolution velocity data are not available.

Acknowledgments
This research was made possible by a grant from the Gulf of Mexico Research Initiative. Data are publicly available through the Gulf of Mexico Research Initiative Information and Data Cooperative (GRIIDC) at https://data.gulfresearchinitiative.org/data/R5.x283.000:0003 (doi:10.7266/n7-rctx-2r57).

References

Belcher, S. E., Grant, ALM., Hanley, K. E., Fox-Kemper, B., Van Roekel, L., Sullivan, P. P., & Polton, J. A. (2012). A global perspective on Langmuir turbulence in the ocean surface boundary layer: Frontier. *Geophysical Research Letters*, *39*, L18605. https://doi.org/10.1029/2012GL052932

Bou-Zeid, E., Meneveau, C., & Parlange, M. (2005). A scale-dependent Lagrangian dynamic model for large eddy simulation of complex turbulent flows. *Physics of Fluids*, *17*(2), 025105. https://doi.org/10.1063/1.1839152

Chamecki, M., Meneveau, C., & Parlange, M. B. (2008). A hybrid spectral/finite-volume algorithm for large-eddy simulation of scalars in the atmospheric boundary layer. *Boundary-Layer Meteorology*, *128*(3), 473–484. https://doi.org/10.1007/s10546-008-9302-1

Chen, B., Yang, D., Meneveau, C., & Chamecki, M. (2016). Effects of swell on transport and dispersion of oil plumes within the ocean mixed layer. *Journal of Geophysical Research: Oceans*, *121*, 3564–3578. https://doi.org/10.1002/2015JC011380

Chen, B., Yang, D., Meneveau, C., & Chamecki, M. (2018). Numerical study of the effects of chemical dispersant on oil transport from an idealized underwater blowout. *Physical Review Fluids*, *3*, 083801. https://doi.org/10.1103/PhysRevFluids.3.083801

Chor, T., Yang, D., Meneveau, C., & Chamecki, M. (2018). Preferential concentration of noninertial buoyant particles in the ocean mixed layer under free convection. *Physical Review Fluids*, *3*, 64501. https://doi.org/10.1103/PhysRevFluids.3.064501

Craik, A. D. D., & Leibovich, S. (1976). A rational model for Langmuir circulations. *Journal of Fluid Mechanics*, *73*(3), 401–426. https://doi.org/10.1017/S0022112076001420

De Bruin, H. A. R., & Bink, N. J. (1994). The use of σT as a temperature scale in the atmospheric surface layer. *Boundary-Layer Meteorology*, *70*(1), 79–93. https://doi.org/10.1007/BF00712524

Donelan, M. A., & Pierson, W. J. (1987). Radar scattering and equilibrium ranges in wind-generated waves with application to scatterometry. *Journal of Geophysical Research*, *92*(C5), 4971–5029.

Esler, J. G., & Ramli, H. M. (2017). Shear dispersion in the turbulent atmospheric boundary layer. *Quarterly Journal of the Royal Meteorological Society*, *143*(705), 1721–1733. https://doi.org/10.1002/qj.3039

Kaimal, J. C., Wyngaard, J. C., Haugen, D. A., Cot, O. R., Izumi, Y., Caughey, S. J., & Readings, C. J. (1976). Turbulence structure in the convective boundary layer. *Journal of the Atmospheric Sciences*, *33*(11), 2152–2169. https://doi.org/10.1175/1520-0469(1976)033<2152:TSITCB>2.0.CO;2

Kukulka, T., & Brunner, K. (2015). Passive buoyant tracers in the ocean surface boundary layer: 1. Influence of equilibrium wind-waves on vertical distributions. *Journal of Geophysical Research: Oceans*, *120*, 3837–3858. https://doi.org/10.1002/2014JC010487

Kukulka, T., Law, K. L., & Proskurowski, G. (2016). Evidence for the influence of surface heat fluxes on turbulent mixing of microplastic marine debris. *Journal of Physical Oceanography*, *46*(3), 809–815. https://doi.org/10.1175/JPO-D-15-0242.1

Kukulka, T., Plueddemann, A. J., & Sullivan, P. P. (2013). Inhibited upper ocean restratification in nonequilibrium swell conditions. *Geophysical Research Letters*, *40*, 3672–3676. https://doi.org/10.1002/grl.50708

Large, W. G., McWilliams, J. C., & Doney, S. C. (1994). Oceanic vertical mixing: A review and a model with a nonlocal boundary layer parameterization. *Reviews of Geophysics*, *32*(4), 363–403. https://doi.org/10.1029/94RG01872

Laxague, N. J. M., Özgökmen, T. M., Haus, B. K., Novelli, G., Shcherbina, A., Sutherland, P., & Molemaker, J. (2018). Observations of near-surface current shear help describe oceanic oil and plastic transport. *Geophysical Research Letters*, *45*, 245–249. https://doi.org/10.1002/2017GL075891

10.1029/2018GL080296

Liang, J. H., Wan, X., Rose, K. A., Sullivan, P. P., & McWilliams, J. C. (2018). Horizontal dispersion of buoyant materials in the ocean surface boundary layer. *Journal of Physical Oceanography*, *48*, 2103–2125. https://doi.org/10.1175/JPO-D-18-0020.1

Lilly, D. K. (1967). The representation of small scale turbulence in numerical simulation experiments. In *Proceedings of the IBM Scientific Computing Symposium on environmental sciences, Yorktown heights* (pp. 195–210).

McWilliams, J. C., & Restrepo, J. M. (1999). The wave-driven ocean circulation. *Journal of Physical Oceanography*, *29*(10), 2523–2540. https://doi.org/10.1175/1520-0485(1999)029<2523:TWDOC>2.0.CO;2

McWilliams, J. C., & Sullivan, P. P. (2000). Vertical mixing by Langmuir circulations. *Spill Science & Technology Bulletin Langmuir Circulation and Oil Spill Modeling*, *6*(3), 225–237. https://doi.org/10.1016/S1353-2561(01)00041-X

McWilliams, J. C., Sullivan, P. P., & Moeng, C. H. (1997). Langmuir turbulence in the ocean. *Journal of Fluid Mechanics*, *334*, 1–30. https://doi.org/10.1017/S0022112096004375

Pearson, B. C., Grant, A. L. M., Polton, J. A., & Belcher, S. E. (2015). Langmuir turbulence and surface heating in the ocean surface boundary layer. *Journal of Physical Oceanography*, *45*(12), 2897–2911. https://doi.org/10.1175/JPO-D-15-0018.1

Smagorinsky, J. (1963). General circulation experiments with the primitive equations. *Monthly Weather Review*, *91*(3), 99–164. https://doi.org/10.1175/1520-0493(1963)091<0099:GCEWTP>2.3.CO;2

Smyth, W. D., Skyllingstad, E. D., Crawford, G. B., & Wijesekera, H. (2002). Nonlocal fluxes and Stokes drift effects in the K-profile parameterization. *Ocean Dynamics*, *52*(3), 104–115. https://doi.org/10.1007/s10236-002-0012-9

Taylor, G. I. (1953). Dispersion of soluble matter in solvent flowing slowly through a tube. *Proceedings of the Royal Society of London A: Mathematical, Physical and Engineering Sciences*, *219*(1137), 186–203. https://doi.org/10.1098/rspa.1953.0139

Taylor, J. R. (2018). Accumulation and subduction of buoyant material at submesoscale fronts. *Journal of Physical Oceanography*, *48*(6), 1233–1241. https://doi.org/10.1175/JPO-D-17-0269.1

Thorpe, S. (2004). Langmuir circulation. *Annual Review of Fluid Mechanics*, *36*(1), 55–79. https://doi.org/10.1146/annurev.fluid.36.052203.071431

Yang, D., Chamecki, M., & Meneveau, C. (2014). Inhibition of oil plume dilution in Langmuir ocean circulation. *Geophysical Research Letters*, *41*, 1632–1638. https://doi.org/10.1002/2014GL059284

Yang, D., Chen, B., Chamecki, M., & Meneveau, C. (2015). Oil plumes and dispersion in Langmuir, upper-ocean turbulence: Large-eddy simulations and K-profile parameterization: LES oil plume dispersion. *Journal of Geophysical Research: Oceans*, *120*, 4729–4759. https://doi.org/10.1002/2014JC010542

Yang, D., Chen, B., Socolofsky, S. A., Chamecki, M., & Meneveau, C. (2016). Large-eddy simulation and parameterization of buoyant plume dynamics in stratified flow. *Journal of Fluid Mechanics*, *794*, 798–833. https://doi.org/10.1017/jfm.2016.191

Zheng, L., & Yapa, P (2000). Buoyant velocity of spherical and nonspherical bubbles/droplets. *Journal of Hydraulic Engineering*, *126*(11), 852–854. https://doi.org/10.1061/(ASCE)0733-9429(2000)126:11(852)

Zilitinkevich, S. (1994). A generalized scaling for convective shear flows. *Boundary-Layer Meteorology*, *70*(1), 51–78. https://doi.org/10.1007/BF00712523